

This discussion paper is/has been under review for the journal Ocean Science (OS).  
Please refer to the corresponding final paper in OS if available.

# Changes in extreme regional sea surface height due to an abrupt weakening of the Atlantic MOC

S.-E. Brunnabend<sup>1</sup>, H. A. Dijkstra<sup>1</sup>, M. A. Kliphuis<sup>1</sup>, B. van Werkhoven<sup>2</sup>, E. Bal<sup>2</sup>,  
F. Seinstra<sup>3</sup>, J. Maassen<sup>3</sup>, and M. van Meersbergen<sup>3</sup>

<sup>1</sup>Institute of Marine and Atmospheric Research Utrecht, Utrecht University, Princetonplein 5,  
3584 CC Utrecht, the Netherlands

<sup>2</sup>Department of Computer Science, VU University Amsterdam, 1081 HV Amsterdam, the  
Netherlands

<sup>3</sup>Netherlands eScience Center, 1098 XG Amsterdam, the Netherlands

Received: 13 March 2014 – Accepted: 10 April 2014 – Published: 30 April 2014

Correspondence to: S.-E. Brunnabend (s.h.brunnabend@uu.nl)

Published by Copernicus Publications on behalf of the European Geosciences Union.

Title Page

Abstract

Introduction

Conclusions

References

Tables

Figures

◀

▶

◀

▶

Back

Close

Full Screen / Esc

Printer-friendly Version

Interactive Discussion



## Abstract

As an extreme scenario of dynamical sea level changes, regional sea surface height (SSH) changes that occur in the North Atlantic due to an abrupt weakening of the Atlantic Meridional Overturning Circulation (AMOC) are simulated. Two versions of the same ocean-only model are used to study the effect of ocean model resolution on these SSH changes: a high-resolution (HR) strongly eddying version and a low-resolution (LR) version in which the effect of eddies are parameterized. The weakening of the AMOC is induced in both model versions by applying strong freshwater perturbations around Greenland. A rapid decrease of the AMOC in the HR version induces much shorter return times of several specific regional and coastal extremes in North Atlantic SSH than in the LR version. This effect is caused by a change in main eddy pathways associated with a change in separation latitude of the Gulf Stream.

## 1 Introduction

The global mean rate of sea level rise over the twentieth century, as deduced from tide gauges, is about  $1.7 \pm 0.5 \text{ mm year}^{-1}$  (Bindoff et al., 2007). However, regional sea level changes have been very inhomogeneous over this period and are affected by changes in atmospheric wind stresses, and surface heat and freshwater fluxes (Ishii et al., 2003; Volkov et al., 2003; Antonov et al., 2005; Bindoff et al., 2007; Berge-Nguyen et al., 2008; Church et al., 2008; Woodworth et al., 2011a). Hence regional sea level change is often associated with variations in ocean circulation (Landerer et al., 2007; Levermann et al., 2005; Flückiger et al., 2006; Stammer, 2008; Stammer et al., 2011; Lorbacher et al., 2010; Hu et al., 2011). Changes in the amount of water in the oceans (barystatic) as well as changes in land water mass distribution, and their gravitational, elastic, and rotational effects (changes in the static-equilibrium) may also affect regional sea level (Farrell and Clark, 1976; Clark et al., 1978; Mitrovica et al., 2001, 2011; Kopp et al., 2010).

OSD

11, 1213–1241, 2014

## Change in regional SSH extremes

S.-E. Brunnabend et al.

Title Page

Abstract

Introduction

Conclusions

References

Tables

Figures

◀

▶

◀

▶

Back

Close

Full Screen / Esc

Printer-friendly Version

Interactive Discussion



**Change in regional SSH extremes**

S.-E. Brunnabend et al.

Title Page

Abstract

Introduction

Conclusions

References

Tables

Figures

◀

▶

◀

▶

Back

Close

Full Screen / Esc

Printer-friendly Version

Interactive Discussion



Changes in regional extreme sea levels have been related mostly to changes in the mean sea level, storm surges and wind setup (Marcos et al., 2009; Lowe et al., 2010; Woodworth et al., 2011b). In a recent study of water levels from tide gauges, Merrifield et al. (2013) identify, apart from tidal and seasonal components, non-tidal residual components as an important contribution to annual maximum water levels. Such non-tidal residuals can result from high-frequency storms and processes on subannual time scales. Firing and Merrifield (2004) indicate, through an example near Hawaii in September 2003, that mesoscale eddies may have an important influence on extreme sea levels. This study describes an eddy that gave rise to extreme sea levels as it coincided with high sea level in both seasonal and longer (decadal) time scale components.

Apart from sea level changes due to gradual background climate changes there is the potential for more rapid and extreme sea level changes due to the sensitivity of the Atlantic Meridional Overturning Circulation (AMOC) to freshwater anomalies (Srokosz et al., 2012). In this case, the large-scale changes in the ocean circulation may lead to large background sea level changes in a few decades. These have to be added to the sea level changes, which are caused by the many other processes on the regional scale.

One of the sources of freshwater input is the mass loss of the Greenland Ice Sheet (GrIS) which is at the moment estimated to be about 0.01 Sv (Mernild et al., 2010). A scenario where GrIS freshwater might modify the AMOC has been considered in different ocean-climate models. These models mostly employ a freshwater inflow of 0.1 Sv and a horizontal resolution of about 1.0° such that the effect of ocean eddies are parameterized. In most of these non-eddy ocean/climate models, the AMOC is weakening in response to this freshwater input. This weakening has a strong dependence on the model resolution, the amount of freshwater inflow and on the region where the freshwater is introduced into to ocean (Gerdes et al., 2006; Stouffer et al., 2006; Stammer, 2008; Kopp et al., 2010; Hu et al., 2011; Stammer et al., 2011; Brunnabend et al., 2012).

**Change in regional  
SSH extremes**

S.-E. Brunnabend et al.

Title Page

Abstract

Introduction

Conclusions

References

Tables

Figures

◀

▶

◀

▶

Back

Close

Full Screen / Esc

Printer-friendly Version

Interactive Discussion



These model studies have indicated that the freshening and the change in the AMOC affect regional sea level in the North Atlantic (Levermann et al., 2005; Flückiger et al., 2006). On multidecadal time scales, the freshwater from the GrIS leads to a sea level response mainly in the North Atlantic. Stammer (2008), using the MITgcm (Marshall et al., 1997), found a decreasing sea level in the subpolar North Atlantic. He attributed this depression to cold water anomalies, an accelerated subpolar gyre and a slow-down of the subtropical gyre. A similar sea level response is also visible in the study of Stammer et al. (2011) where a coupled ocean–atmosphere model is used. The study by Hu et al. (2011) estimates the potential of mass loss of the GrIS under different climate scenarios using the Climate System Model version 3 (CCSM3, Collins et al., 2006). The resulting dynamic sea level change does not show a this significant signal. Only a slightly negative signal south of Island is visible, which disappears under a warmer background climate. The simulations of Wang et al. (2012) and Brunnabend et al. (2012) were performed using the finite element sea-ice ocean model (FESOM, Sidorenko et al., 2011). With a more realistic GrIS freshwater perturbation (Brunnabend et al., 2012), only a reduced sea level increase is visible in the subpolar North Atlantic.

Recently, such a hosing simulation was performed with a strongly eddying ocean model. In Weijer et al. (2012), the transient multidecadal time scale response of the AMOC due to 0.1 Sv of freshwater inflow at the Greenland coast was determined using the Parallel Ocean Program (POP) model. Both the magnitude of the response as well as the mechanisms of AMOC decline are different in the strongly eddying model than in the non-eddying version of the POP (Den Toom et al., 2014). The low-resolution model results show a change of the net freshwater advection that is consistent with the salt advection feedback. However, for the eddy-resolving model, the net freshwater advection into the Atlantic basin appears to be unaffected, despite the significant change in the large-scale velocity structure.

The main aim of this study is to investigate the impact of an abrupt AMOC decline due to GrIS freshwater input on extremes in regional sea surface height in the North Atlantic. The interesting aspect is that a large change in the AMOC potentially can lead

to changes in the spatio-temporal properties of the eddy field and hence may affect regional extremes in sea level. In Sect. 2, the model and the simulations performed are discussed. Using a similar approach as in Weijer et al. (2012) and Den Toom et al. (2014), we compare the AMOC and sea surface height responses to GrIS freshwater perturbations in both a non-eddyding and a strongly eddyding version of the same ocean model (POP) in Sect. 3. In Sect. 4, extreme value theory is applied on sea surface height data (regional and coastal) to determine changes in extremes associated with the AMOC changes (and freshening) in the North Atlantic. In Sect. 5, a summary and discussion is provided.

## 2 Model and simulations

Simulations were performed using the global Los Alamos Parallel Ocean Program (POP) (Maltrud et al., 2008), forced by monthly atmospheric climatology data (CORE I; Large and Yeager, 2004). The high-resolution model, here referred to as HR, has a spatial resolution of  $0.1^\circ$  horizontally and has 42 depth levels. The horizontal grid allows to represent eddies and a detailed boundary current behavior, such as an adequate separation of the Gulf Stream (Maltrud et al., 2008). In the low-resolution version of the POP model, referred to as the LR version, the grid has a horizontal resolution of  $1.0^\circ$  and has 40 depth levels. The eddy-induced transports are parameterized. As described in Weijer et al. (2012), mixed boundary conditions are used in both model versions where the prescribed freshwater flux is derived from an earlier restoring simulation (hence in the simulations discussed below, there is no salinity and temperature restoring applied). Further details about the spin-up, forcing and simulations with both versions of the POP model can be found in the Supplement of Weijer et al. (2012).

In both LR and HR versions, a prognostic implicit free-surface formulation is used where the sea surface height  $\eta$  is solved from a linearized free surface model. Following (Landerer et al., 2007), we will refer to  $\eta$  as the dynamic sea surface height (SSH). Because the freshwater forcing is represented as a virtual salt flux, no net

## Change in regional SSH extremes

S.-E. Brunnabend et al.

Title Page

Abstract

Introduction

Conclusions

References

Tables

Figures



Back

Close

Full Screen / Esc

Printer-friendly Version

Interactive Discussion



**Change in regional SSH extremes**

S.-E. Brunnabend et al.

Title Page

Abstract

Introduction

Conclusions

References

Tables

Figures

I◀

▶I

◀

▶

Back

Close

Full Screen / Esc

Printer-friendly Version

Interactive Discussion



global changes in the precipitation-evaporation+river runoff can occur and hence no barystatic changes are represented. The variations in SSH can be decomposed into contributions from bottom pressure changes and steric height variations (the barometric correction is zero). The spatially homogeneous (but time-dependent) global steric contribution can be determined from the ocean model output in a post-processing step (Greatbatch, 1994). However, the global mean steric contribution originating from additional freshwater inflow around Greenland appears to be one order of magnitude smaller than the corresponding global mean mass contribution (Brunnabend et al., 2012). Hence it is not considered here.

Apart from a control simulation, with no additional freshwater inflow around Greenland and hence with constant salt content in the ocean, two 50 year simulations are performed with both the LR and HR model versions. In the first simulation, an additional 0.1 Sv is added around Greenland and in the second simulation 0.5 Sv is added. The freshwater inflow around Greenland has a seasonal dependence with maximum amplitudes in July. The spatial distribution of the freshwater input, as shown in Fig. 1 of Weijer et al. (2012), is based on observations of calving and runoff derived by Rignot and Kanagaratnam (2006). This distribution includes a high rate of freshwater inflow near southeast and west Greenland and no inflow in the southwest. Lower rates are located at the northern and northeast coast of Greenland.

In the results below, SSH changes are computed by taking the difference between a model simulation, including the additional freshwater inflow, and the control simulation. Before analysis, the data from the LR and HR simulation has been interpolated to a regular  $0.4^\circ$  horizontal longitude-latitude grid. As extremes in sea level for area-averaged quantities are investigated, this interpolation has no influence on the results. When considering coastal SSH extremes, locations are used that are at the same point as in the  $0.1^\circ$  grid to make sure no systematic inflation of extremes occur.

### 3 Results

#### 3.1 Flow changes

The maximum of the annual mean AMOC at 35° N (the approximate latitude of the overall maximum) for the LR and HR control simulations, the HR 0.1 Sv simulation, and the HR and LR 0.5 Sv simulations are plotted in Fig. 1a. The strength of the AMOC at 35° N for the HR 0.0 Sv simulation slightly increases and equilibrates to an annual average of about 25 Sv in 50 years. For both HR 0.1 and 0.5 Sv simulations, the strength of the AMOC decreases to values of about 18 Sv and 11 Sv, respectively, at year 50. The effect of the extra freshwater perturbation near Greenland can be more explicitly seen in Fig. 1b, where the differences to the control simulation are plotted. For the HR 0.5 Sv case, a reduction of about 14 Sv occurs over 50 year of simulation. The pattern of the AMOC remains the same during its weakening and there is no collapse to a different equilibrium (Den Toom et al., 2014). The overturning cell weakens due to the additional freshwater input near Greenland and the reverse bottom cell slightly strengthens. The same holds for the LR 0.5 Sv simulation results (Den Toom et al., 2014).

In Fig. 2a and b, the annual mean of the surface horizontal velocity field in the North Atlantic for both LR and HR control simulations, respectively, is shown at year 1. While the overall surface current patterns are similar in both versions of the model, the boundary layer currents are more narrow and the flow is much less spatially coherent in the HR version. The annual mean surface horizontal velocity field difference between the 0.5 Sv perturbed simulation and control simulation at year 50 is plotted for the LR and HR versions in Fig. 2c and 2d, respectively. Strong qualitative differences between the model results occur in the Gulf Stream region and the subpolar gyre. Changes in surface speeds are up to 1 ms<sup>-1</sup> in the HR version. They are much smaller in the LR version.

In the HR model, a northward shift in the latitude of the Gulf Stream separation occurs after about 25 years (Fig. 3b). During the last decade of the 0.5 Sv model simulation the position of the Gulf Stream separation stabilizes at a level around 37° N.

Title Page

Abstract

Introduction

Conclusions

References

Tables

Figures

◀

▶

◀

▶

Back

Close

Full Screen / Esc

Printer-friendly Version

Interactive Discussion



**Change in regional SSH extremes**

S.-E. Brunnabend et al.

Title Page

Abstract

Introduction

Conclusions

References

Tables

Figures

◀

▶

◀

▶

Back

Close

Full Screen / Esc

Printer-friendly Version

Interactive Discussion



The separation latitude in the control run remains in the interval [35° N, 35.5° N]. Although the latitude position of the Gulf Stream separation is already located too far north in the LR control simulation, a similar shift as in the HR simulation is also found (Fig. 3a). The shift is caused by the modification of the lateral density gradient over the Gulf Stream due to the freshening. This leads to a change in the Rossby deformation radius affecting eddy formation and through rectification processes, to a weakening of the Gulf Stream core near the separation latitude (Fig. 2d). Consequently, the decrease of inertia causes a less sharp separation and a northward deflection of the jet.

The change in salinity after 50 years due to the 0.5 Sv input of freshwater is shown in Fig. 4. In the LR simulation (Fig. 4a), the freshwater anomalies travel southward along the western boundary of the North Atlantic until they encounter the Gulf Stream. From this latitude the anomaly is transported eastward and follows a path along the subtropical gyre. The main difference to this description in the HR simulation is that the freshwater anomaly is more homogeneous due to the mixing effect of the eddies (Fig. 4b). Similarly, the changes in temperature are plotted in Fig. 4c and d. While both model versions show a cooling in the subtropical gyre, it is much stronger in the HR simulation. In the LR simulation, the shift in the Gulf Stream path causes a warm anomaly south of the main current (Fig. 4c) which is not seen in the HR simulation (Fig. 4d).

The cause of the strong cooling in the subpolar gyre in the HR simulation can be attributed to the changes in the northward surface currents as can be seen clearly in the change in eddy kinetic energy after 30 and 50 years (Fig. 5). For the 0.5 Sv simulation (Fig. 5c and d), there is a change in the path of the North Atlantic current, from a northward oriented component to a more eastward oriented component. As a consequence, less heat is transported northwards which cools the subpolar gyre. For the 0.1 Sv HR simulation a similar spatial structure change can be seen (Fig. 5a and b) but of weaker amplitude.

## 3.2 Sea surface height changes

Figure 6a and b show the near equilibrium (annual mean) SSH at the start of the fresh-water perturbation for the LR and HR configurations, respectively. The pattern and amplitude in Fig. 6a compares well with that in other coarse resolution models (compare this result to e.g. Fig. 1b in Landerer et al., 2007). The pattern in Fig. 6b compares very well with that of the CMDT-RIO03 model of dynamic topography (Rio and Hernandez, 2004, see e.g. Fig. 1a in Landerer et al., 2007) having more detailed spatial variations in the western boundary current regions than in Fig. 6a. Over 50 years, modeled SSH for the 0.5 Sv simulation mainly changes in the North Atlantic, as shown in Fig. 6c (LR) and d (HR). Although the patterns are overall similar, Fig. 6d provides much more spatial detail as it also includes the eddy-induced small-scale SSH changes. The difference in SSH change between Fig. 6c and d is particularly striking in the subpolar gyre. In the HR simulation, a SSH decrease occurs whereas a weak SSH increase is found in the LR simulation.

In general, the temporal evolution of the pattern of SSH change in the North Atlantic caused by the additional freshwater agrees well with other studies (Stammer, 2008; Hu et al., 2011; Wang et al., 2012; Brunnabend et al., 2012). During the first years, SSH mainly changes in the area of the Labrador Sea and Baffin Bay. As freshwater is transported by the western boundary currents, SSH rises near the North American coast. In the following years the freshwater is transported eastward where it separates and distributes to the Arctic Ocean as well as to the equatorial Atlantic. The corresponding halo-steric expansion leads SSH to rise in the freshened regions. In addition, there are changes in the circulation pattern, and consequently in the eddy pathways (Fig. 5), in the North Atlantic that are leading to additional variations in regional SSH. The SSH changes are therefore different in the LR and HR models as they depend on the capability of the ocean model to represent ocean eddies.

OSD

11, 1213–1241, 2014

## Change in regional SSH extremes

S.-E. Brunnabend et al.

Title Page

Abstract

Introduction

Conclusions

References

Tables

Figures

◀

▶

◀

▶

Back

Close

Full Screen / Esc

Printer-friendly Version

Interactive Discussion



## 4 Changes in sea surface height extremes

To analyze regional extremes in SSH anomalies, monthly mean SSH in three different regions (indicated in Fig. 7a) in the North Atlantic are determined. The regions are chosen as they represent areas of major SSH change (Fig. 6), i.e. the SSH decrease in the subpolar gyre (region 1), and the increase in SSH in the western (region 2) and eastern (region 3) North Atlantic.

For the HR 0.5 Sv simulation, the area-averaged perturbed SSHP (SSHP = SSH hosing – SSH control) in region 1 shows (blue curve in Fig. 7b), after an initial increase, a decrease over the 50 year period. After about 40 years, the SSHP has stabilized and shows only a seasonal cycle; the short time scale variability, visible during the first 30 years, has disappeared. This behavior can be explained by the shift in the horizontal velocities as shown in Fig. 2 and the reduction of the eddy kinetic energy (Fig. 5c and d) in this region. It indicates that at later times eddies do not propagate into the region anymore.

Similar stabilization behavior is visible in the region near the European coast (blue curve in Fig. 7d), where SSHP increases, but a clear seasonal cycle is absent. At the North American coast, the SSHP continues to rise over the simulation period (blue curve in Fig. 7c). In Fig. 7 also the SSH changes due to a 0.1 Sv GrIS perturbation are shown as red curves (the gaps are due to missing data values, see Supplement of Weijer et al., 2012). The same sign of the trends is found as for the 0.5 Sv simulation, but the responses are weaker.

To investigate variations in extremes of the SSHP that are induced by changes in the eddy fields, we subtract the area-averaged SSHP (as in Fig. 7) of a region from the monthly-mean SSHP fields. Then the linear trend at each location in the region is removed and the maximum SSHP value (of the region) is determined for each month. The extreme SSHP values obtained over the first ten model years (model years 1–10) are then compared with those over the last decade (model years 41–50) by determining parameters in the Generalized Extreme Value distribution based on 120 data points

Title Page

Abstract

Introduction

Conclusions

References

Tables

Figures

◀

▶

◀

▶

Back

Close

Full Screen / Esc

Printer-friendly Version

Interactive Discussion



(months). Parameters are fitted by maximum likelihood estimates of the parameters of the GEV distribution following (Coles, 2001).

For the 0.1 Sv HR simulation, the return period of an extreme of 1 m in region 1 (subpolar gyre) decreases from being longer than 500 months to 200 months (Fig. 8a).

5 In region 2 (western Atlantic), the SSHP extreme corresponding to the 100 months return period remains similar in time as this region mainly undergoes a change in the mean SSHP (Fig. 8b). In region 3 (eastern Atlantic), the extreme corresponding to a 100 months return period decreases by about 10 cm (Fig. 8c). For the 0.5 GrIS perturbed HR simulation, the return periods in region 1 (subpolar gyre, Fig. 8d) are decreasing for extreme values having an initial return period of 100 months or less. However, the return periods of 1 m of SSHP are becoming similar again. In the other two regions, much larger extremes are caused by more intense eddies and the shift in their flow direction. The extreme corresponding to a 100 month return period increases by 0.5 m in region 2 (Fig. 8e), and in region 3, the return period for a SSH change of 10  
15 0.8 m is decreased to about 100 months (Fig. 8f).

The results for the 0.5 Sv LR simulation (Fig. 9) show similar qualitative differences (between the blue and green curves) in SSHP extremes for all three regions but the changes in the extreme SSHP values are much smaller. In contrast to the HR results, the curves flatten also for higher return times. This indicates that the changes in eddy paths (Fig. 2d) are the cause of the higher values of the extremes in the HR simulation. In the LR model, these effects are not captured as only large-scale changes in SSH can be represented.

At four coastal locations (Azores, Lisbon, New York, and Bermuda Islands) daily SSH changes due to the freshwater perturbation around Greenland are plotted in Fig. 10. The long-term changes mainly result from the reduced salinity in these regions. At the coast near New York, SSHP shows a strong increase in the first 3 years which is caused by the reduced salinity near the east coast of North America during that time period. Near Lisbon, for example, SSHP only slightly increases until the freshwater has actually arrived in this region after about one decade.

## Change in regional SSH extremes

S.-E. Brunnabend et al.

Title Page

Abstract

Introduction

Conclusions

References

Tables

Figures

◀

▶

◀

▶

Back

Close

Full Screen / Esc

Printer-friendly Version

Interactive Discussion



**Change in regional SSH extremes**

S.-E. Brunnabend et al.

[Title Page](#)[Abstract](#)[Introduction](#)[Conclusions](#)[References](#)[Tables](#)[Figures](#)[◀](#)[▶](#)[◀](#)[▶](#)[Back](#)[Close](#)[Full Screen / Esc](#)[Printer-friendly Version](#)[Interactive Discussion](#)

The changes in coastal SSH extremes are computed by identifying the maximum SSHP of every month from daily mean data at the four coastal locations. Before, the long-term signal has been removed from the daily time series to consider only short-term variations, i.e., those caused by high-frequency variations in the flow, for example due to eddies. The return times of extremes in SSHP of the first ten years of the model simulation (green curves in Fig. 11) are next compared to those of the last ten years (blue curves in Fig. 11). At the European coast an increase in short-term extremes of about 10 cm (Azores) and 5 cm (Lisbon) for a return period of 100 months is visible. The return times of short-term extremes remain similar at the Bermuda Islands, whereas the amplitude of the extremes for every return time near the coast near New York are decreased.

## 5 Summary, discussion and conclusion

The SSH response after 50 years of freshwater input near Greenland in both strongly-eddy (HR) and non-eddy (LR) ocean-only model (POP) configurations has been investigated in this study. The large freshwater perturbations (0.1 Sv and 0.5 Sv) are unrealistic as a near-future scenario for freshwater input into the North Atlantic and were only used to cause the decrease in the AMOC.

Sea level changes due to both freshwater input and flow changes are found in both models. A comparison between LR and HR model versions shows that high spatial resolution is of major importance when investigating regional dynamic sea level changes in the North Atlantic. The detailed flow changes in the surface velocity field in the HR simulation can lead to large scale SSH changes which are qualitatively very different from the LR model results, for example in the subpolar gyre.

The differences between the 0.1 Sv and 0.5 Sv HR model responses are mostly quantitative. A freshwater inflow of 0.1 Sv shows similar response patterns in the velocity field and in SSH as in the 0.5 Sv results. The signal to noise ratio is, however, much smaller in the 0.1 Sv case. This is in good agreement with other studies, e.g.

Kopp et al. (2010) and Brunnabend et al. (2012), which have shown that an increase in the amount of freshwater perturbation leads to an increased amplitude in SSH change while the pattern remains fairly similar.

The study by Firing and Merrifield (2004) showed that when investigating local extremes in sea level, eddies can further enhance short-term sea level extremes and that return times of these extremes decrease with rise in mean sea level. By focusing only on the monthly-mean maxima and by filtering out the longer time scale effects, changes in short-term extremes of local SSH due to flow changes can be studied. For the 0.5 Sv HR simulation, a change in the spatial pattern of the eddy field especially near the coasts of Europe is found. This leads to an additional regional increase in SSH of several centimeters. Also the return period of regional extremes that are caused by the changing eddy field is reduced in different coastal regions, causing more frequent extreme sea levels. The shift of the eddy kinetic energy distribution is not as pronounced in the 0.1 Sv as in the 0.5 Sv simulation and eddies have a smaller influence on SSH extremes in near coastal regions during the investigated period of time.

In reality, the AMOC may be much more sensitive to freshwater perturbations than in the POP model considered here (Smeed et al., 2013). The HR POP version is not in a multiple equilibrium regime (Den Toom et al., 2014) and hence the AMOC does not collapse to a different equilibrium state. When the AMOC is in a multiple equilibrium regime, it may actually decrease within a few decades (Hawkins et al., 2011), even under much smaller freshwater perturbations. In this case variations in eddy paths can provide an additional component of sea level change which can strongly affect regional and local extremes. So far this component was not considered, as it is not represented in LR ocean-climate models, but in future scenarios of coastal sea level change where the extreme scenario of AMOC changes is considered, it should be taken into account.

*Acknowledgements.* The project is supported by the Netherlands eScience Center (NLeSC) via the project eSALSA (An eScience Approach to determine future Sea-level chAnGes). The simulations have been performed on the Huygens IBM Power6 supercomputer at SURFsara

**Change in regional SSH extremes**

S.-E. Brunnabend et al.

Title Page

Abstract

Introduction

Conclusions

References

Tables

Figures

◀

▶

◀

▶

Back

Close

Full Screen / Esc

Printer-friendly Version

Interactive Discussion



(<https://www.surfsara.nl>) through the project SH-243-13. We thank Leela Frankcombe for providing the scripts to compute the separation latitude of the Gulf Stream.

## References

- Antonov, J. I., Levitus, S., and Boyer, T. P.: Thermosteric sea level rise, 1955–2003, *Geophys. Res. Lett.*, 32, I12602, doi:10.1029/2005GL023112, 2005. 1214
- 5 Berge-Nguyen, M., Cazenave, A., Lombard, A., Liovel, W., Viarra, J., and Cretaux, J. F.: Reconstruction of past decades sea level using thermosteric sea level, tide gauge, satellite altimetry and ocean reanalysis data, *Global Planet. Change*, 62, 1–13, doi:10.1016/j.gloplacha.2007.11.007, 2008. 1214
- 10 Bindoff, N. L., Willebrand, J., Artale, V., Cazenave, A., Gregory, J., Gulev, S., Hanawa, K., Le Quéréand, C., Levitus, S., Nojiri, Y., Shum, C. K., Talley, L. D., and Unnikrishnan, A.: Observations: Oceanic Climate Change and Sea Level, in: *The Scientific Basis, Contribution of Working Group I to the Fourth Assessment Report of the Intergovernmental Panel on Climate Change*, edited by Solomon, S., Qin, D., Manning, M., Chen, Z., Marquis, M., Averyt, K. B., Tignor, M., and Miller, H. L., Cambridge University Press, Cambridge, New York, 2007. 1214
- 15 Brunnabend, S.-E., Schröter, J., Timmermann, R., Rietbroek, R., and Kusche, J.: Modeled steric and mass-driven sea level change caused by Greenland Ice Sheet melting, *J. Geodyn.*, 59–60, 219–225, doi:10.1016/j.jog.2011.06.001, 2012. 1215, 1216, 1218, 1221, 1225
- 20 Church, J. A., White, N. J., Aarup, T., Wilson, W. S., Woodworth, P. L., Domingues, C. M., Hunter, J. R., and Lambeck, K.: Understanding global sea levels: past, present and future, *Sustain. Sci.*, 3, 9–22, doi:10.1007/s11625-008-0042-4, 2008. 1214
- Clark, J. A., Farrell, W. E., and Peltier, W. R.: Global changes in postglacial sea level: a numerical calculation, *Quaternary Res.*, 9, 265–287, 1978. 1214
- 25 Coles, S.: *An Introduction to Statistical Modeling of Extreme Values*, Springer-Verlag London Ltd, 2001. 1223
- Collins, W. D., Bitz, C., Blackmon, M. L., Bonan, G., Bretherton, C. S., Carton, J. A., Chang, P., Doney, S. C., Hack, J. J., Henderson, T. B., Kiehl, J. T., Large, W. G., McKenna, D. S., Santer, B. D., and Smith, R. D.: The Community Climate System Model Version 3 (CCSM3), *J. Climate*, 19, 2122–2143, doi:10.1175/JCLI3761.1, 2006. 1216
- 30

## Change in regional SSH extremes

S.-E. Brunnabend et al.

[Title Page](#)
[Abstract](#)
[Introduction](#)
[Conclusions](#)
[References](#)
[Tables](#)
[Figures](#)
[◀](#)
[▶](#)
[◀](#)
[▶](#)
[Back](#)
[Close](#)
[Full Screen / Esc](#)
[Printer-friendly Version](#)
[Interactive Discussion](#)


- Den Toom, M., Dijkstra, H. A., Weijer, W., Hecht, M. W., and Maltrud, M. E.: Sensitivity of a strongly eddying global ocean to North Atlantic freshwater perturbations, *J. Phys. Oceanogr.*, 44, 464–481, 2014. 1216, 1217, 1219, 1225
- Farrell, W. E. and Clark, J. A.: On postglacial sea level, *Geophys. J. Roy. Astr. S.*, 46, 647–667, doi:10.1111/j.1365-246X.1976.tb01252.x, 1976. 1214
- Firing, Y. L. and Merrifield, M. A.: Extreme sea level events at Hawaii: influence of mesoscale eddies, *Geophys. Res. Lett.*, 31, L24306 doi:10.1029/2004GL021539, 2004. 1215, 1225
- Flückiger, J., Knutti, R., and White, J. W. C.: Oceanic processes as potential trigger and amplifying mechanisms for Heinrich events, *Paleoceanography*, 21, pA2014 doi:10.1029/2005PA001204, 2006. 1214, 1216
- Gerdes, R., Hurlin, W., and Griffies, S. M.: Sensitivity of a global ocean model to increased runoff from Greenland, *Ocean Model.*, 12, 416–435, doi:10.1016/j.ocemod.2005.08.003, 2006. 1215
- Greatbatch, R. J.: A note on the representation of steric sea level in models that conserve volume rather than mass, *J. Geophys. Res.*, 99, 12767–12771, 1994. 1218
- Hawkins, E., Smith, R. S., Allison, L. C., Gregory, J. M., Woollings, T. J., Pohlmann, H., and De Cuevas, B.: Bistability of the Atlantic overturning circulation in a global climate model and links to ocean freshwater transport, *Geophys. Res. Lett.*, 38, L10605, doi:10.1029/2011GL047208, 2011. 1225
- Hu, A., Meehl, G. A., Han, W., and Yin, J.: Effect of the potential melting of the Greenland Ice Sheet on the meridional overturning circulation and global climate in the future, *Deep-Sea Res. Pt. II*, 58, 1914–1926, doi:10.1016/j.dsr2.2010.10.069, 2011. 1214, 1215, 1216, 1221
- Ishii, M., Kimoto, M., and Kaci, M.: Historical ocean subsurface temperature analysis with error estimates, *Mon. Weather Rev.*, 131, 51–73, 2003. 1214
- Kopp, R. E., Mitrovica, J. X., Griffies, S. M., Yin, J., Hay, C. C., and Stouffer, R. J.: The impact of Greenland melt on local sea levels: a partially coupled analysis of dynamic and static equilibrium effects in idealized water-hosing experiments, *Climate Change*, 103, 619–625, doi:10.1007/s10584-010-9935-1, 2010. 1214, 1215, 1225
- Landerer, F. W., Jungclaus, J. H., and Marotzke, J.: Regional dynamic and steric sea level change in response to the IPCC-A1B scenario, *J. Phys. Oceanogr.*, 37, 296–312, doi:10.1175/JPO3013.1, 2007. 1214, 1217, 1221
- Large, W. G. and Yeager, S. G.: Diurnal to decadal global forcing for ocean and sea-ice models; the datasets and flux climatologies, NCAR Technical Note TN 460 STR, available at:

<http://www.clivar.org/organization/wgomd/resources/core/core-i> (last access: October 2008), 2004. 1217

Levermann, A., Griesel, A., Hofmann, M., Montoya, M., and Rahmstorf, S.: Dynamic sea level changes following changes in the thermohaline circulation, *Clim. Dynam.*, 24, 347–354, doi:10.1007/s00382-004-0505-y, 2005. 1214, 1216

Lorbacher, K., Dengg, J., Böning, C. W., and Biastoch, A.: Regional patterns of sea level change related to interannual variability and multidecadal trends in the Atlantic meridional overturning circulation, *J. Climate*, 23, 4243–4254, doi:10.1175/2010JCLI3341.1, 2010. 1214

Lowe, J. A., Woodworth, P. L., Knutson, T., McDonald, R. E., McInnes, K. L., With, K., von Storch, H., Wolf, J., Swail, V., Bernier, N. B., Gulev, S., Horsburgh, K. J., Unnikrishnan, A. S., Hunter, J. R., and Wiese, R.: Past and future change in extreme sea levels and waves, in: *Understanding Sea-Level Rise and Variability*, edited by: Church, J. A., Woodworth, P. L., Aarup, T., and Wilson, W. S., Wiley, Blackwell, UK, 326–375, 2010. 1215

Maltrud, M., Bryan, F., Hecht, M., Hunke, E., Ivanova, D., McClean, J., and Peacock, S.: Global ocean modeling in the eddying regime using POP, *CLIVAR Exchange*, 44, 5–8, 2008. 1217

Marcos, M., Tsimplis, M. N., and Shaw, A. G. P.: Sea level extremes in southern Europe, *J. Geophys. Res.*, 114, c01007 doi:10.1029/2008JC004912, 2009. 1215

Marshall, J., Adcroft, A., Hill, C., Perelman, L., and Heisey, C.: A finite-volume, incompressible Navier–Stokes model for studies of the ocean on parallel computers, *J. Geophys. Res.*, 102, 5753–5766, doi:10.1029/96JC02775, 1997. 1216

Mernild, S. H., Liston, G. E., Hiemstra, C. A., and Christensen, J. H.: Greenland Ice Sheet surface mass-balance modeling in a 131-yr perspective, 1950–2080, *J. Hydrometeorol.*, 11, 3–25, doi:10.1175/2009JHM1140.1, 2010. 1215

Merrifield, M. A., Genz, A. S., Kontoes, C. P., and Marra, J. J.: Annual maximum water levels from tide gauges: Contribution factors and geographic patterns, *J. Geophys. Res.-Oceans*, 118, 2535–2546, doi:10.1002/jgrc.20173, 2013. 1215

Mitrovica, J. X., Tamisiea, M. E., Davis, J. L., and Milne, G. A.: Recent mass balance of polar ice sheets inferred from patterns of global sea-level change, *Nature*, 409, 1026–1029, 2001. 1214

Mitrovica, J. X., Gomez, N., Morrow, E., Hay, C., Latychev, K., and Tamisiea, M. E.: On the robustness of predictions of sea level fingerprints, *Geophys. J. Int.*, 197, 729–742, doi:10.1111/j.1365-246X.2011.05090.x, 2011. 1214

## Change in regional SSH extremes

S.-E. Brunnabend et al.

Title Page

Abstract

Introduction

Conclusions

References

Tables

Figures

◀

▶

◀

▶

Back

Close

Full Screen / Esc

Printer-friendly Version

Interactive Discussion



## Change in regional SSH extremes

S.-E. Brunnabend et al.

[Title Page](#)
[Abstract](#)
[Introduction](#)
[Conclusions](#)
[References](#)
[Tables](#)
[Figures](#)
[Back](#)
[Close](#)
[Full Screen / Esc](#)
[Printer-friendly Version](#)
[Interactive Discussion](#)


- Rignot, E. and Kanagaratnam, P.: Changes in the velocity structure of the Greenland Ice Sheet, *Science*, 311, 986–990, doi:10.1126/science.1121381, 2006. 1218
- Rio, M.-H. and Hernandez, F.: A mean dynamic topography computed over the world ocean from altimetry, in-situ measurements and a geoid model, *J. Geophys. Res.*, 109, c12032 doi:10.1029/2003JC002226, 2004. 1221
- Sidorenko, D., Wang, Q., Danilov, S., and Schröter, J.: FESOM under coordinated ocean-ice reference experiment forcing, *Ocean Dynam.*, 61, 881–890, doi:10.1007/s10236-011-0406-7, 2011. 1216
- Smeed, D. A., McCarthy, G. D., Cunningham, S. A., Frajka-Williams, E., Rayner, D., Johns, W. E., Meinen, C. S., Baringer, M. O., Moat, B. I., Duchez, A., and Bryden, H. L.: Observed decline of the Atlantic meridional overturning circulation 2004–2012, *Ocean Sci.*, 10, 29–38, doi:10.5194/os-10-29-2014, 2014. 1225
- Srokosz, M., Baringer, M., Bryden, H., Cunningham, S., Delworth, T., Lozier, S., Marotzke, J., and Sutton, R.: Past, present, and future changes in the Atlantic meridional overturning circulation, *B. Am. Meteorol. Soc.*, 93, 1663–1676, doi:10.1175/BAMS-D-11-00151.1, 2012. 1215
- Stammer, D.: Response of the global ocean to Greenland and Antarctic ice melting, *J. Geophys. Res.*, 113, c06022, doi:10.1029/2006JC004079, 2008. 1214, 1215, 1216, 1221
- Stammer, D., Agarwal, N., Herrmann, P., Köhl, A., and Mechoso, C. R.: Response of a coupled ocean-atmosphere model to Greenland ice melting, *Surv. Geophys.*, 32, 621–642, doi:10.1007/s10712-011-9142-2, 2011. 1214, 1215, 1216
- Stouffer, R. J., Yin, J., Gregory, J. M., Dixon, K. W., Spelman, M. J., Hurlin, W., Weaver, A. J., Eby, M., Flato, G. M., Hasumi, H., Hu, A., Jungclaus, J. H., Kamenkovich, I. V., Levermann, A., Montoya, M., Murakami, S., Nawrath, S., Oka, A., Peltier, W. R., Robitaille, D. Y., Sokolov, A., Vettoretti, G., and Waber, S. L.: Investigating the causes of the response of the thermohaline circulation to past and future climate changes, *J. Climate*, 19, 1365–1387, doi:10.1175/JCLI3689.1, 2006. 1215
- Volkov, D. L., Hendrik, M., and van Aken, H. W.: Annual and inter annual variability of sea level in the northern North Atlantic Ocean, *J. Geophys. Res.*, 108, 3204, doi:10.1029/2002JC001459, 2003. 1214
- Wang, X., Wang, Q., Sidorenko, D., Danilov, S., Schröter, J., and Jung, T.: Long-term ocean simulations in FESOM: evaluation and application in studying the impact of Greenland Ice Sheet melting, *Ocean Dynam.*, 62, 1471–1486, doi:10.1007/s10236-012-0572-2, 2012. 1216, 1221

- Weijer, W., Maltrud, M. E., Hecht, M. W., Dijkstra, H. A., and Kliphuis, M. A.: Response of the Atlantic Ocean circulation to Greenland Ice Sheet melting in a strongly-eddy ocean model, *Geophys. Res. Lett.*, 39, I09606, doi:10.1029/2012GL051611, 2012. 1216, 1217, 1218, 1222
- 5 Woodworth, P. L., Gehrels, W. R., and Nerem, R. S.: Nineteenth and twentieth century changes in sea level, *Oceanography*, 24, 80–93, doi:10.5670/oceanog.2011.29, 2011a. 1214
- Woodworth, P. L., Menéndez, M., and Gehrels, W. R.: Evidence for century-timescale acceleration in mean sea levels and for recent changes in extreme sea levels, *Surv. Geophys.*, 32, 603–618, doi:10.1007/s10712-011-9112-8, 2011b. 1215

**Change in regional SSH extremes**

S.-E. Brunnabend et al.

Title Page

Abstract

Introduction

Conclusions

References

Tables

Figures

◀

▶

◀

▶

Back

Close

Full Screen / Esc

Printer-friendly Version

Interactive Discussion



## Change in regional SSH extremes

S.-E. Brunnabend et al.

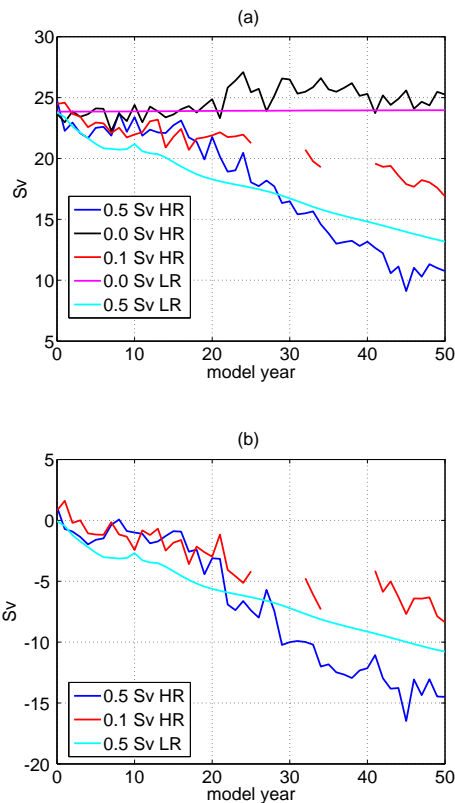


**Fig. 1.** (a) Strength of the Atlantic Meridional Overturning (AMOC) at 35° N for the HR control simulation (black), the LR control simulation (magenta), the 0.1 Sv HR simulation (red, the gaps are due to missing data), the 0.5 Sv HR simulation (blue) and the LR 0.5 Sv simulation (light blue). (b) AMOC anomalies (with respect to the control simulation) of the different perturbed simulations (same color coding as in a).

Title Page

Abstract

Introduction

Conclusions

References

Tables

Figures

◀

▶

◀

▶

Back

Close

Full Screen / Esc

Printer-friendly Version

Interactive Discussion



Change in regional  
SSH extremes

S.-E. Brunnabend et al.

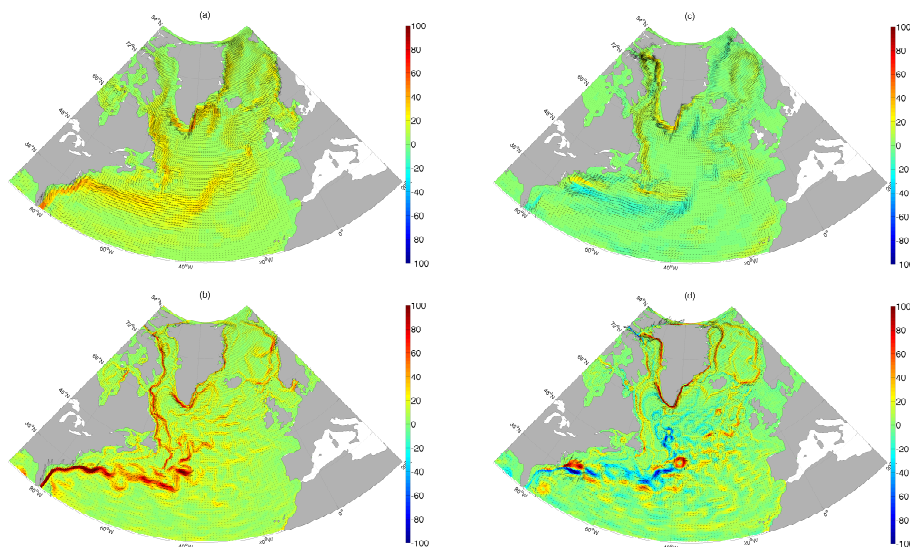


**Fig. 2.** Horizontal velocity vector field and speed (in  $\text{cm s}^{-1}$ ) of the control run **(a)** of the LR simulation and **(b)** the HR simulation; changes of the horizontal velocity structure caused by the 0.5 Sv perturbation after 50 model years **(c)** of the LR simulation and **(d)** of the HR simulation.

[Title Page](#)[Abstract](#)[Introduction](#)[Conclusions](#)[References](#)[Tables](#)[Figures](#)[◀](#)[▶](#)[◀](#)[▶](#)[Back](#)[Close](#)[Full Screen / Esc](#)[Printer-friendly Version](#)[Interactive Discussion](#)

## Change in regional SSH extremes

S.-E. Brunnabend et al.

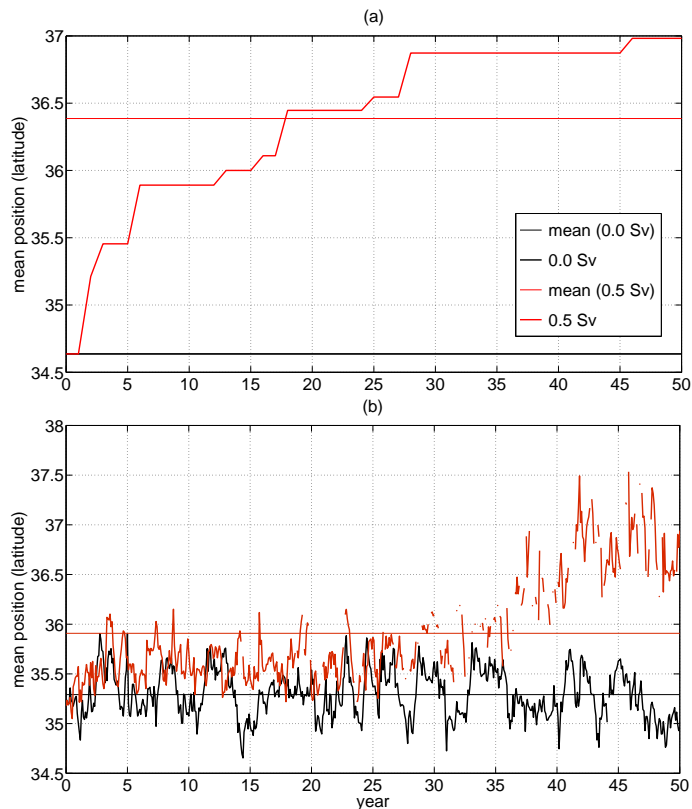


**Fig. 3.** (a) Latitudinal position of the Gulf Stream separation from the LR model simulation (black) and the 0.5 Sv perturbation simulation (red). It is computed by identifying the path of the Gulf Stream from yearly-mean sea surface height (SSH) data. Next the separation latitude is defined as the mean latitude position within the interval [76–70° W]. The horizontal lines indicate the mean position of both time series. (b) Same as in (a) but for the HR 0.5 Sv simulation (monthly mean SSH data used).

Change in regional  
SSH extremes

S.-E. Brunnabend et al.

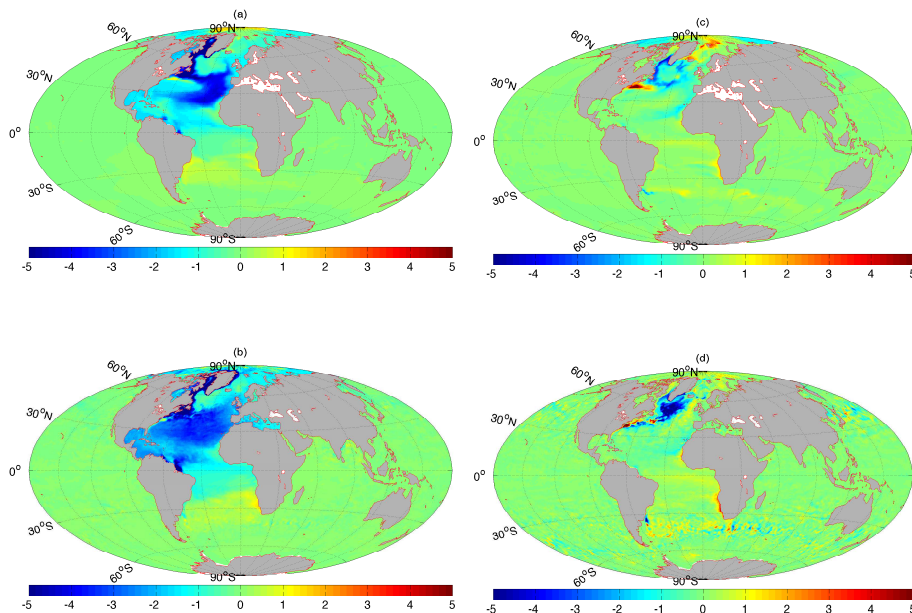


**Fig. 4.** (a–b) Change in sea surface salinity (in psu) after 50 years due to the input of 0.5 Sv freshwater around Greenland in the (a) LR and (b) HR simulations. (c–d) Change in sea surface temperature (in °C) due to the input of 0.5 Sv freshwater around Greenland for the (c) LR and (d) HR simulations.

Title Page

Abstract

Introduction

Conclusions

References

Tables

Figures

◀

▶

◀

▶

Back

Close

Full Screen / Esc

Printer-friendly Version

Interactive Discussion



Change in regional  
SSH extremes

S.-E. Brunnabend et al.

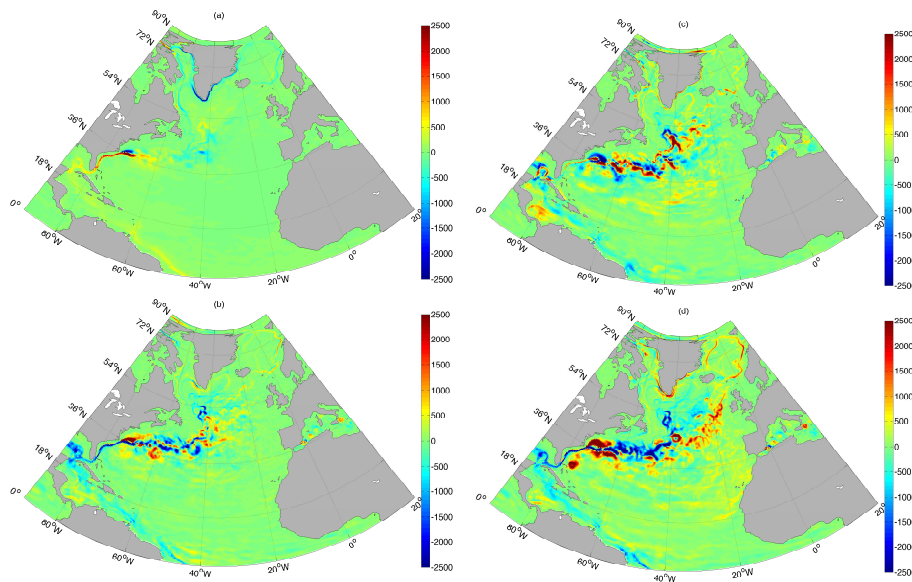


**Fig. 5.** Eddy Kinetic Energy (EKE) changes ( $\text{cm}^2 \text{s}^{-2}$ ) for the HR 0.1 Sv (**a, b**) and 0.5 Sv (**c, d**) perturbations after 30 (**a, c**) and 50 (**b, d**) years.

Title Page

Abstract

Introduction

Conclusions

References

Tables

Figures

◀

▶

◀

▶

Back

Close

Full Screen / Esc

Printer-friendly Version

Interactive Discussion



## Change in regional SSH extremes

S.-E. Brunnabend et al.

Title Page

Abstract

Introduction

Conclusions

References

Tables

Figures

◀

▶

◀

▶

Back

Close

Full Screen / Esc

Printer-friendly Version

Interactive Discussion

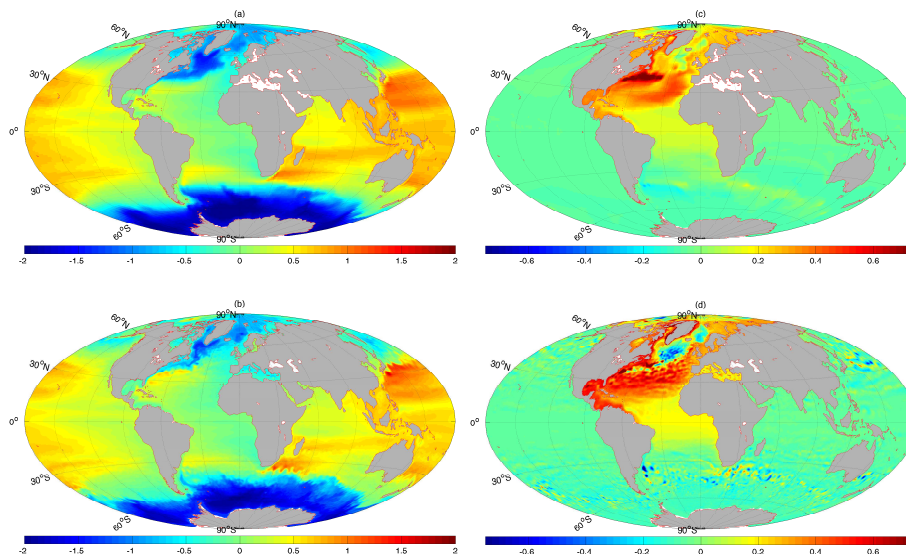


**Fig. 6.** (a) Annual mean sea surface height (SSH, in m) at the start of the freshwater release in the LR model. (b) Same as (a) but for the HR model. (c) Change in SSH (hosing – control) after 50 years due to a 0.5 Sv of freshwater inflow around Greenland in the LR model. (d) Same as (c) but for the HR model.

## Change in regional SSH extremes

S.-E. Brunnabend et al.

Title Page

Abstract

Introduction

Conclusions

References

Tables

Figures

◀

▶

◀

▶

Back

Close

Full Screen / Esc

Printer-friendly Version

Interactive Discussion

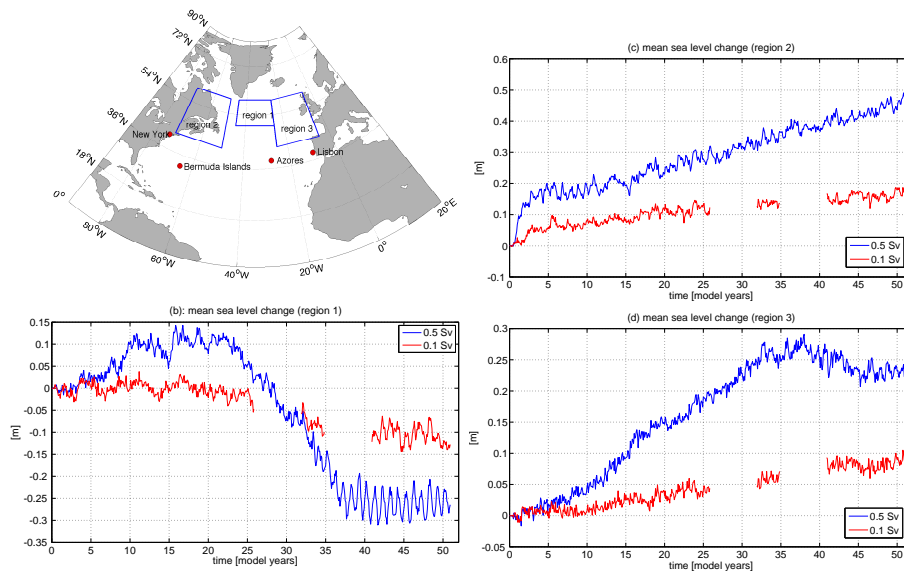


**Fig. 7.** (a) Location of three areas and coastal positions of interest. (b–d) Area-averaged SSH change (hosing – control) as determined from the simulations with the HR model for the 0.1 Sv GrIS perturbation (red curves) and the 0.5 Sv GrIS perturbation (blue curves), of (b) region 1, (c) region 2, (d) region 3.

## Change in regional SSH extremes

S.-E. Brunnabend et al.

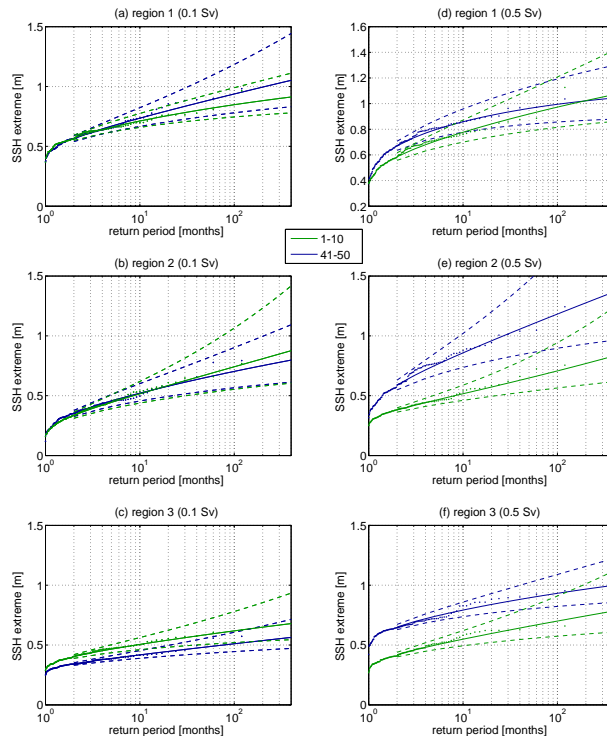


**Fig. 8.** Generalized Extreme Value (GEV) distribution fits to monthly maximum SSHP changes in the different regions. **(a–c)** GEV plots for the 0.1 Sv HR simulation. **(d–f)** GEV plots for the 0.5 Sv HR simulation. The extreme values are plotted as a function of return times using 10 years of data at the beginning of the simulation (green: years 1–10) and for a similar period at the end of the simulation (blue: 41–50). The dashed curves indicate the 95% confidence interval corresponding to the GEV fit. The area-averaged mean (shown in Fig. 7b–d) of the each region is subtracted and then the linear trend at each location in a region is removed before determining the extreme values.

[Title Page](#)
[Abstract](#)
[Introduction](#)
[Conclusions](#)
[References](#)
[Tables](#)
[Figures](#)
[◀](#)
[▶](#)
[◀](#)
[▶](#)
[Back](#)
[Close](#)
[Full Screen / Esc](#)
[Printer-friendly Version](#)
[Interactive Discussion](#)

## Change in regional SSH extremes

S.-E. Brunnabend et al.

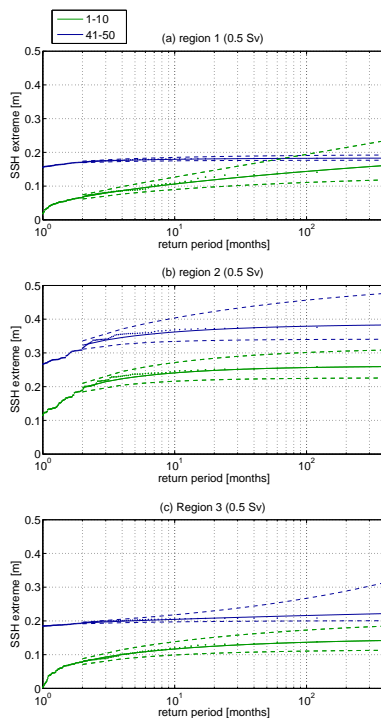


**Fig. 9.** Generalized Extreme Value (GEV) distribution fits to monthly maximum sea SSH changes in the different regions; **(a–c)** GEV plots for the 0.5 Sv LR simulation. The extreme values are plotted as a function of return times using 10 years of data at the beginning of the simulation (green: years 1–10) and for a similar period at the end of the simulation (blue: 41–50). The dashed curves indicate the 95 % confidence interval corresponding to the GEV fit. The area-averaged mean of the each region is subtracted and then the linear trend at each location in a region is removed before determining the extreme values.

Title Page

Abstract

Introduction

Conclusions

References

Tables

Figures

◀

▶

◀

▶

Back

Close

Full Screen / Esc

Printer-friendly Version

Interactive Discussion



## Change in regional SSH extremes

S.-E. Brunnabend et al.

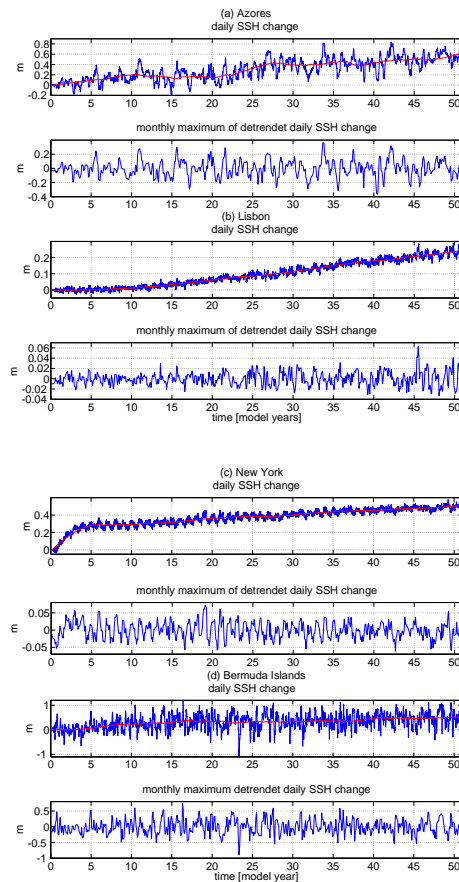


**Fig. 10. (a–d)** Monthly maximum values of daily SSHP change at a coastal location (blue) with its long term signal (red) and the monthly maximum of the high pass filtered (detrended) daily mean SSHP change. The locations considered are **(a)**: Azores, **(b)**: Lisbon, **(c)**: New York and **(d)**: Bermuda Islands.

Title Page

Abstract

Introduction

Conclusions

References

Tables

Figures

◀

▶

◀

▶

Back

Close

Full Screen / Esc

Printer-friendly Version

Interactive Discussion



## Change in regional SSH extremes

S.-E. Brunnabend et al.

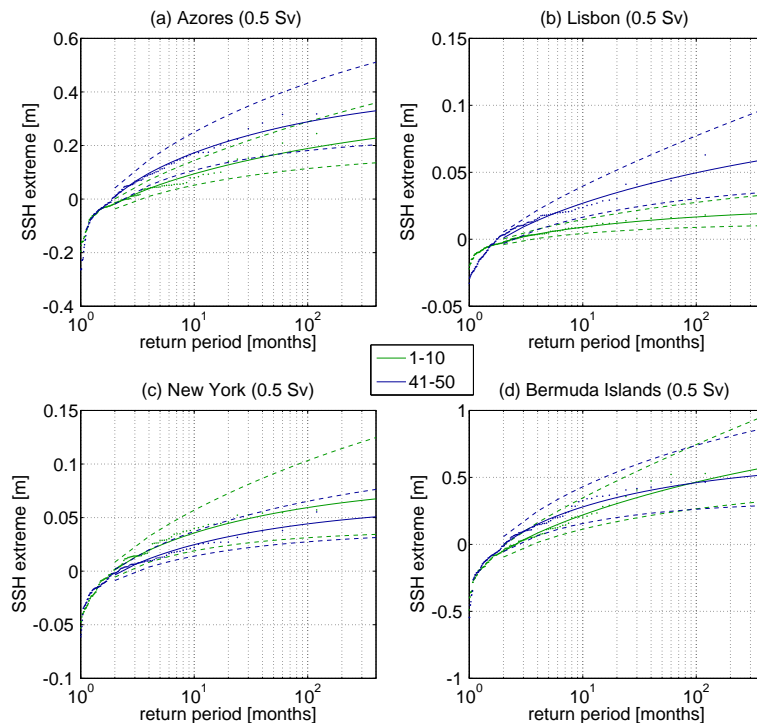


**Fig. 11.** Generalized Extreme Value (GEV) distribution fits to monthly maxima of detrended daily SSHP changes in the different coastal locations in the North Atlantic for the 0.5 Sv HR simulation. The extreme values are plotted as a function of return times using 10 years of data at the beginning of the simulation (green: years 1–10) and for a similar period at the end of the simulation (blue: 41–50). The dashed curves indicate the 95% confidence interval corresponding to the GEV fit. The locations considered are **(a)**: Azores, **(b)**: Lisbon, **(c)**: New York and **(d)**: Bermuda Islands.

Title Page

Abstract

Introduction

Conclusions

References

Tables

Figures

◀

▶

◀

▶

Back

Close

Full Screen / Esc

Printer-friendly Version

Interactive Discussion

